THE ASTROPHYSICAL JOURNAL, 321:496–515, 1987 October 1

DOPPLER IMAGES OF ROTATING STARS USING MAXIMUM ENTROPY IMAGE RECONSTRUCTION[1]

STEVEN S. VOGT, G. DONALD PENROD, AND ARTIE P. HATZES
Lick Observatory, Board of Studies in Astronomy and Astrophysics, University of California, Santa Cruz
Received 1987 January 23; accepted 1987 March 17

ABSTRACT

We present an improved version of the Doppler imaging technique, which now uses the principles of maximum entropy image reconstruction to derive spatially resolved images of rapidly rotating stars. We examine the effects that noise, finite spectral resolution, and uncertain stellar parameters are likely to have on real data sets, and demonstrate through a variety of test cases that the technique is efficient and accurate at recovering test images from realistic synthetic spectral data. At the high signal-to-noise ratio and resolution typical of our real stellar spectra, the images are well constrained by the data set alone, rather than by entropy criteria. We are currently using the technique to study cool starspots on RS CVn and FK Com stars, and the surface abundance distributions on Ap stars.

Subject headings: line profiles — stars: peculiar A — stars: rotation

I. INTRODUCTION

Several years ago, we described a technique, Doppler imaging, for obtaining resolved images of certain rapidly rotating late-type spotted stars (Vogt and Penrod 1982, 1983). This technique exploits the correspondence between wavelength position across a rotationally broadened spectral line and spatial position across the stellar disk. Basically, cool spots on the surface of a rapidly rotating star produce distortions in the star's spectral lines. If the star is spinning rapidly enough so that the shape of its spectral line profiles are dominated by rotational Doppler broadening, a high degree of correlation exists between the position of any distortion within a line profile and the position of the corresponding spot on the stellar surface. In such a case, a high-resolution spectrum is essentially a one-dimensional image of the star, completely blurred in latitude. As the star is viewed from other aspects (i.e., at different rotation phases), other one-dimensional images can be obtained. Then, if the rotation period and inclination are well known, all the one-dimensional images can in principle be assembled into a two-dimensional image of the stellar surface.

The major difficulty in carrying out the Doppler imaging technique is, of course, how to "invert" the line profiles. That is, how to map distortions in the line profiles back on to the star in such a way as to produce a unique map of the star. The task of predicting spectral line flux profiles which would be produced by a rotating star with a *known* spot configuration is relatively straightforward. It simply requires an integration of appropriate specific intensity spectral line profiles and velocity fields across the stellar disk. However, the problem at hand is the inverse of this, working backward from a set of observed spectral line profiles to get the brightness distribution across the disk. There is, in principle, no unique solution to the inversion problem.

This "inverse" problem has in the past been encountered by a number of researchers attempting to map the distributions of chemical abundances on the surfaces of Ap stars from observed spectral variations. Deutsch (1958, 1970) described a method, called harmonic analysis, in which the distribution of local equivalent width on the surface of the star was represented as a series expansion of spherical harmonics. A similar expansion was made of the observed radial velocity and magnetic field variations. A system of equations was then set up which could be solved analytically for the expansion coefficients. A major drawback and fundamental limitation of the harmonic analysis technique is that, in order to obtain an analytic solution to the equations, the expansion series must be truncated after only a few terms. This severely restricts the type of features which can be discerned and the level of spatial detail in the resultant image. Also the Deutsch technique used only the *integral* characteristics of the line profiles. For slowly rotating stars, where the line profiles contain no spatial information, this is adequate. But, for rapidly rotating stars where spatial detail is mapped into the line profiles through rotational line broadening, one needs a method which can extract spatial information from the *shapes* of the line profiles, and preferably without any ad hoc assumptions about the nature of the features to be imaged.

Several attempts were made to improve on the harmonic approach by correcting the problem of using the integrated line characteristics. Pyper (1969) and Megessier (1975) divided the spectral line into components and identified spots on the stellar surface responsible for each of the components of the line. However, work by Pavlova, Khokhlova, and Aslanov (1977) showed that this was subject to arbitrariness and produced unpredictable errors. Falk and Wehlau (1974) added information about the line profiles to the technique by using a series expansion of the residual intensities at each frequency of the line profile. However, their approach used an unrealistic assumption of a Gaussian intrinsic profile which is constant across the disk. Although the harmonic analysis technique may have been improved by using the information in the line shapes, it still suffered from the handicap of having the series expansion truncated to a few terms to keep the equations tractable. Thus information in the line profile shapes could be lost by virtue of the technique's inability to discern complex spatial features on the star.

Khokhlova also realized that any successful inversion technique must use the information contained in the line profile shapes. Her first attempts at solving the inverse problem of

[1] *Lick Observatory Bulletin* No. 1066.

obtaining abundance maps from line profile variations were by trial and error (Khokhlova 1975; Khokhlova and Rayabchikova 1975). The technique employed was similar to that used by Vogt and Penrod (1983) for imaging the late-type star HR 1099. An initial guess was made as to the sizes and locations of features of enhanced abundance on a hypothetical star. The integrated line profile as a function of phase from this distribution was then compared to the actual data. Appropriate changes to the original distribution were then made, and the process repeated until an adequate fit to the data was obtained. This technique suffered from the obvious drawback in that it was highly subjective and time-consuming.

Goncharsky *et al.* (1982) developed an algorithm for deriving a map of the local equivalent width using only the observed line profiles. They represented the observed spectral lines by an integral equation of the local equivalent width integrated over the stellar disk and used regularizing algorithms to solve for the local equivalent width map. The intrinsic local line profiles were represented using Voigt profiles for the absorption coefficient and the Minnaert approximation to the equation of transfer.

The Goncharsky technique was applied to several Ap stars by Khokhlova (1985) and most recently by Khokhlova, Rice, and Wehlau (1986), yielding abundance distributions of varying degrees of complexity. The simplest maps showed one or two spots, while the most complex consisted of up to six spots. However, the work of Khokhlova and co-workers generally failed to recover any latitude information about the spots, as their solutions were always strongly biased to the sub-observer latitude on the star.

It was clear from inspection of our line profiles of spotted late-type stars, that a much higher degree of spatial structure was present than any of the various existing line profile inversion methods could handle. Also previous techniques were unable to obtain accurate latitude information on spot distributions. This is quite unacceptable for imaging spotted late-type stars since the spot locations are always changing and it is hoped that, by imaging these stars, we can follow spot migration motions in latitude as well as longitude. Since none of these previous methods for inverting spectral line data seemed well suited for Doppler imaging of spotted late-type stars, we started by working the problem forward. As mentioned previously, our initial approach (Vogt and Penrod 1983) involved simply guessing at the spot distribution and synthesizing the resultant line flux profiles for comparison with the observed data. Then, corrections were made to the initial image and iteration done until all the line profile fits looked reasonable. While this approach clearly worked at some level, it required much time and effort, and it gave no estimate of the degree of nonuniqueness of the final image solution. Also, we were not making complete use of all the information contained in the line profiles, nor were we using information about the noise characteristics of the data. So while this initial approach was successful in producing a Doppler Image, it was clearly unsatisfactory as a general technique for imaging rotating stars.

We have now found a much better method for solving the line profile inversion problem. The technique incorporates the principles of maximum entropy image reconstruction and is proving to be quite robust, efficient, and accurate at producing images of certain classes of rotating stars. The purpose of this paper is to describe the maximum entropy version of Doppler imaging, and to illustrate its power and limitations with some numerical simulations. Application of the Doppler imaging technique to spotted RS CVn stars and Ap stars will be presented in forthcoming papers.

II. REQUIREMENTS FOR DOPPLER IMAGING

a) The Star

In order to obtain a meaningful Doppler image of a star, several criteria must be met. Most importantly, the star must be rotating fast enough so that rotational broadening is the dominant broadening agent of the star's spectral lines. To first order, the number of resolution elements across the disk will be $\approx 2v \sin i/W$, where $v \sin i$ is the projected equatorial rotational velocity, and W is the full width at half-maximum of the line profile which would be measured in the absence of rotation. For spotted late-type dwarfs and subgiants, W is typically of order 10 km s^{-1} for our lines of interest. Thus a minimum $v \sin i$ of at least 20–30 km s^{-1} is needed to get any useful amount of resolution across the surface. In principle, the larger the $v \sin i$, the better the resolution that can be obtained. However, since line equivalent width is, to first order, conserved under rotational broadening, a given line will become shallower as the rotational broadening is increased. Thus, higher S/N or a stronger spectral line will be required in order to detect and accurately measure the distortions in the line profiles. At some level, even with noiseless data, it becomes very difficult to disentangle real profile distortions caused by spots from the myriad of weak unknown terrestrial and stellar line blends in the spectrum. An upper limit of $\sim$80–100 km s^{-1} seems practical at present for late-type stars. For stars with less blended lines, much higher $v \sin i$'s are, of course, usable.

The stellar inclination should also be at an intermediate value. If $i = 0°$, there are no line-of-sight velocity components and thus no possibility of Doppler imaging. If $i = 90°$, there is complete ambiguity as to which hemisphere (north or south) a surface feature is on. This north-south ambiguity results in a Doppler image with mirror-image symmetry about the stellar equator. For large inclinations ($i \geq 70°$), this mirroring will always be a problem. Doppler images are still possible and perhaps useful at these inclinations, but will be harder to interpret. The inclination should thus be in the 20°–70° range for best results. Ideally, the value of the inclination should be well known, but this is a number which is unavailable for many stars. Fortunately, as will be shown, the Doppler imaging technique is fairly insensitive to errors in the assumed inclination.

The physical properties of the stellar atmosphere must also be known. Again, the procedure is fairly insensitive to the detailed physics of the line formation, as long as the observed line profile is dominated by rotational broadening, and an LTE–atmosphere level of approach to the line profile synthesis is an adequate approximation. The variation of continuum brightness and line equivalent width as a function of limb angle must, of course, be treated explicitly in the line flux profile synthesis.

b) The Data Set

The required data set consists of a number of high-resolution, high signal-to-noise ratio spectral line flux profiles, obtained at different rotation phases. The lines can be all of the same transition in a given element or can be a mixture of different lines from the same or different elements. Mixing the lines makes the inversion process slightly more complicated, but may provide more constraints on the image solution if the lines are chosen appropriately. To take fullest advantage of the spatial resolution offered by the stellar rotation, the instrumental profile should not be larger than the star's intrinsic line width. For the spotted late-type stars, a resolution of at least 40,000 is best, although useful information can still be obtained at somewhat lower resolutions.

The amplitude of line profile distortions is generally quite small, typically only about 1% of the continuum. Thus, the spectral data must be of high signal-to-noise ratio. A minimum S/N of at least 100 per resolution element is necessary, but the higher the better. We typically aim for $S/N \geq 400$ per resolution element. The data should also be as free as possible from gross flat-fielding errors and contamination by line blends. Blends can arise both from stellar lines, and from terrestrial lines. Although in practice one picks spectral regions that are as free from blends as possible, it is nearly impossible to completely avoid them. In some of our best spotted star cases, for example, the spotted star is in a binary system, and the lines of the companion star are of comparable strength to those of the spotted star. At certain phases, the lines from the secondary overlap the spotted star's lines and would produce spurious features in the images if not removed completely. Weak terrestrial features are also a concern, though somewhat less troublesome since their positions relative to the line of interest are not phase-locked to the stellar rotation. The line profile software does a good job of differentiating them from the line profile distortions caused by real features on the star (which *are* strictly phase-locked). However, it is advisable to remove the terrestrial features as well as possible by using observations of featureless comparison star spectra at the same airmass. We use spectra of rapidly rotating early-type stars for this.

For a complete and uniquely defined image of the star, a number of spectral line profiles fairly evenly distributed in rotational phase are necessary. Any single line profile gives only a one-dimensional marginal brightness distribution of the star, so observations at many phases are required to give reliable two-dimensional spatial information. In practice, a minimum of eight to 10 observations spread evenly over rotational phase space are needed for a good image. Doppler images with less phase coverage, or uneven coverage of the phase space, may still be useful, but will become incomplete and nonunique.

III. INVERSION OF THE LINE PROFILES

The inversion task is basically a deprojection problem, and such problems are usually best handled numerically in matrix form on a computer. One then has an *image* space and a *data* space, and some matrix which transforms between them in one direction. In our case the image space is the grid of surface brightnesses on the star, and the data space is our set of observed spectral line flux profiles obtained at various phases with a high-resolution spectrometer. The matrix which transforms from image space to data space corresponds to the calculations one goes through to synthesize a spectral line flux profile from a star with known stellar atmosphere and known geometry.

Casting the problem in matrix form, $\boldsymbol{IR} = \boldsymbol{D}$, where $\boldsymbol{I}$ and $\boldsymbol{D}$ are the image and data vectors and $\boldsymbol{R}$ the transfer matrix between the two quantities. Mathematically, this equation can be solved directly for the image vector by finding the inverse of matrix $\boldsymbol{R}$. Then $\boldsymbol{I} = \boldsymbol{DR}^{-1}$. In practice however, this cannot be done. For $\boldsymbol{R}$ to be invertable, not only must the matrix be square, but the m rows of $\boldsymbol{R}$ must be independent. A number of effects such as projection along chords of constant radial velocity, nonzero width of the star's intrinsic line profiles, finite instrumental resolution, incomplete phase coverage, and phase smearing during exposures all contribute to ensure that the rows are not independent. Even if $\boldsymbol{R}$ were directly invertable, this approach may be problematical since the data are always of finite signal-to-noise ratio and thus contain inherent uncertainty. Any noise bumps in the data set would give rise to spurious features in the image.

What is needed is a way to iteratively transform between image and data space, searching among all possible image vectors until one is found which fits all the observed data to within the known noise level of those data. The number of possible image vectors consistent with the data set can be large, and one must set some criterion for selecting the "best" solution. One likely criterion is to choose the simplest or smoothest image, i.e., the one with the least amount of information, which is still consistent with all the data to within the known noise level of the data.

This type of problem is commonly referred to as digital image reconstruction and is often encountered in radio astronomy and in medical imaging. A number of techniques have been developed for reconstructing an image from an incomplete and noisy data set. In 1983, while visiting Lick Observatory, Dr. Keith Horne brought to our attention the existence of a very powerful tool for this type of problem and suggested that it may be very well suited to our particular application. This is the maximum entropy method (Skilling and Bryan 1984 and references therein), realized in software as MEMSYS, a computer program developed by Drs. J. Skilling and S. F. Gull. Of the various known digital image reconstruction techniques, maximum entropy has been shown to be the *optimal* technique of image reconstruction, and the *only* consistent regularization technique for images (Shore and Johnson 1980, 1983; Gull and Skilling 1983). In addition, the MEMSYS implementation of image reconstruction has proven to be extremely robust and efficient and has seen wide application in astronomy, medical imaging, forensic imaging, and elsewhere. Subsequently, the MEMSYS software was kindly made available to us by Dr. Gull through Dr. R. Padman of the U.C. Berkeley Radio Astronomy Laboratory.

Maximum entropy image reconstruction involves finding the image with the greatest configuration entropy:

$$S = -\sum_j p_j \log(p_j) ,$$

where p_j is a normalized *positive* dimensionless image quantity (surface brightness in our case) of the jth image pixel, and the sum is taken over all n image pixels. The maximum entropy image is the one with the least amount of spatial information, and is thus the smoothest or simplest image. In our case, the "smoothest" image means the one with the least contrast between spots and stellar photosphere. An immaculate star, with no spots, will thus be the image with the maximum entropy, but it will not fit the observed line profiles of a spotted star. MEMSYS uses a multidimensional search algorithm to find its maximum entropy image subject to the additional constraint that the image produces data which fit all the real data to within some level ${\chi^2}_0$ where χ^2 is a measure of the misfit:

$$\chi^2 = \sum_k (g_k - d_k)^2/{\sigma_k}^2 .$$

Here g_k is the data set produced by the image solution and d_k are the actual data, whose uncertainty at any point are σ_k.

MEMSYS accomplishes the constrained maximization by the method of Lagrange multipliers, using $\boldsymbol{R}$ and its transpose $\boldsymbol{R}'$ to iterate back and forth between image and data space, seeking to maximize the functional:

$$Q = S - \lambda\chi^2 ,$$

where λ is the Lagrange multiplier. It accomplishes its search very efficiently through the use of conjugate gradient techniques and a six-dimensional subspace of search directions, rather than doing simple line searches. For linear image reconstruction problems, surfaces of constant χ^2 are convex ellipsoids in N-dimensional image space. Since the entropy surfaces are strictly convex, the maximum entropy reconstruction is thus unique (Skilling and Bryan 1984).

In practice, the S/N in our actual line profile data is so high that the image solution is well defined by the χ^2 term only. That is, by the time the iteration has succeeded in fitting the data to the required level of accuracy, further improvements in maximizing the entropy have no appreciable effect on the image. Thus our Doppler images are well constrained by the data set alone and do not rely heavily on entropy considerations. To the level allowed by the data's inherent noise, they are thus unique.

The maximum entropy image is particularly informative and useful since, because it has minimum configurational information, one is assured that any structure present in the image is actually *required* by the data. There may well be finer structure present in the true image, but you will never know it uniquely from your data set. Thus, the signal-to-noise ratio and the quantity of data ultimately determine the level of unique detail allowed in the reconstructed image, as it must. The data can tell you no more.

So the basic task at hand is to set up our imaging problem in a form that is compatible with the MEMSYS codes. This requires an image space which is a one-dimensional vector of n positive image quantities, and a data space which is a one-dimensional vector of m data values (with a specified uncertainty at each point).

a) Defining the Image and Data Vectors

We first define an image vector by dividing the star up into n approximately equal area zones, using the zone geometry shown in Figure 1. The surface is divided up into a grid of zones whose edges lie along lines of latitude and longitude, in such a way as to keep the true area of each zone roughly equal. Thus the zones at high latitudes cover a larger range in longitude than those near the equator. We then represent the stellar disk as a simple one-dimensional *image* vector $\boldsymbol{I}_j$, where each value I_j represents the surface brightness of zone j, for $j = 1$ to n. The value of n is constrained by the desire to adequately resolve the stellar disk while at the same time keeping the problem of manageable size for our VAX 11/780. With typically 10 resolution elements across the disk, zone sizes near the equator of about 5° in longitude by 5° in latitude are sufficient

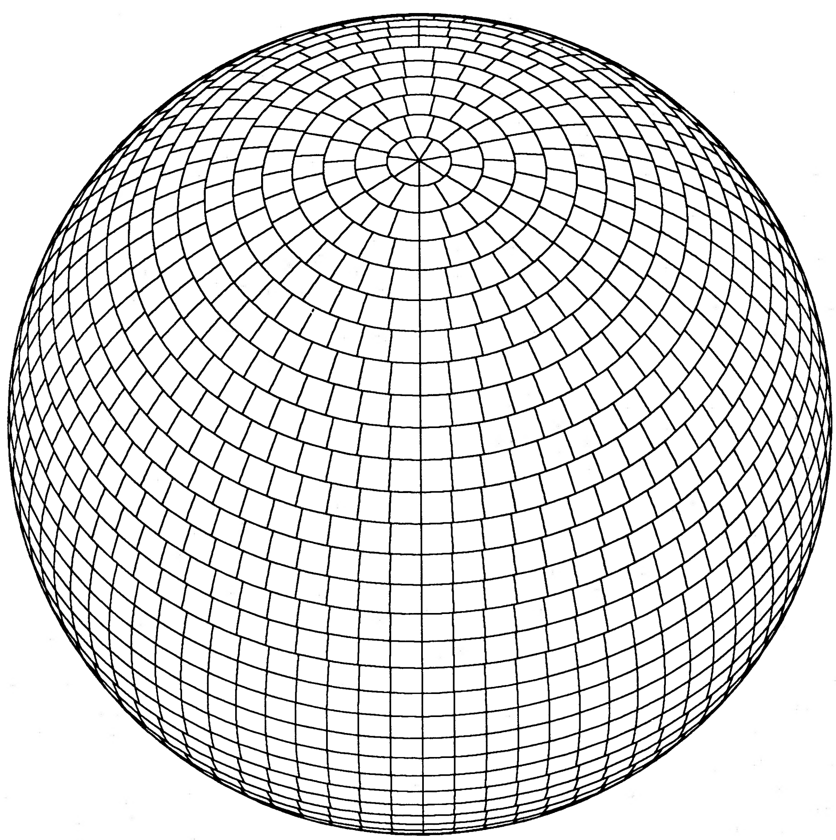

FIG. 1.—Zonal division of the stellar surface. The surface is divided up into 40 latitude bands. At this inclination of 40°, a total of 2310 zones are required to cover the visible portion of the star. Each zone is assigned a corresponding surface brightness. The set of all such surface brightnesses comprises our one-dimensional image vector.

to adequately sample the stellar disk, so in practice n is typically 1200–2500.

The reduced spectral line profiles, with atmospheric and stellar blends carefully removed, are then assembled end-to-end into a one-dimensional data vector D_k, where $k = 1$ to m, with m typically of order 500–1000. The value of m is determined by both the availability of data and again by the desire to keep the transformation matrices of manageable size for our VAX. The line profiles are assembled with just enough room between each phase to reach the local continuum intensity.

b) *Calculating the Response Function Matrix*

We then set up the response function matrix $\boldsymbol{R}$ that relates all the elements in the image vector to all the elements in the data vector. This is done by working the problem *forward* using LTE stellar atmosphere physics and knowledge of the system geometry to set up a system of $m \approx 1000$ equations of $n \approx 2000$ terms each, relating the approximately 1000 data points produced by the spectrometer to the approximately 2000 values of surface brightness on the star:

$$I_1 R_{11} + I_2 R_{21} + \cdots + I_n R_{n1} = D_1$$
$$I_1 R_{12} + I_2 R_{22} + \cdots + I_2 R_{n2} = D_2$$
$$\cdot \quad \cdot \quad \cdot$$
$$\cdot \quad \cdot \quad \cdot$$
$$\cdot \quad \cdot \quad \cdot$$
$$I_1 R_{1m} + I_2 R_{2m} + \cdots + I_n R_{nm} = D_m$$

or

$$\boldsymbol{IR} = \boldsymbol{D}.$$

The matrix $\boldsymbol{R}$ represents the *response* of our measurement apparatus, i.e., a high-resolution spectrometer which measures stellar flux profiles and is situated at some inclination with respect to the star's rotation axis, working at a particular wavelength, and observing at a specific set of rotation phases. In a sense, $\boldsymbol{R}$ is analogous to the point-spread function of an imaging system. Each $\boldsymbol{R}_{jk} = \partial D_k / \partial I_j$ and represents the response of datum pixel k to changes in the surface brightness of image zone j. The $\boldsymbol{R}$ matrix is of course n by m in size, so for our typical cases, with $n \approx 2000$ and $m \approx 1000$, it requires (in byte form) about 2 megabytes of memory.

The continuum intensity and intrinsic shape of the spectral line profile from any localized spot on the star are both functions of limb angle. We first calculate the local specific intensity profiles for 30 limb angles using the ATLAS 5 subroutines from Kurucz (1979) and model atmospheres from a variety of sources. For the RS CVn stars, we use the atmospheres of Bell, *et al.* (1976). The profiles are then convolved with a typical radial-tangential macroturbulent velocity function and with the instrumental profile.

At different phases, a typical zone on the stellar surface will have different (1) projected area, (2) limb angle, and (3) radial velocity (due to stellar rotation). Since we want to know how changing the surface brightness in a given zone will affect the observed rotationally broadened profile at each phase, each of these quantities must be calculated for each zone at each phase. At each phase, the program first calculates the x-y position on the stellar disk corresponding to each latitude-longitude zone. At many phases (if the zone is not circumpolar) a given zone will be on the back side of the star and will not be visible. The effective areas of these zones are set equal to zero. For the zones that are visible, the limb angle is calculated. This then tells the code both which set of specific intensities to use and the projected effective area of that zone at that phase.

For simplicity, we assume that the shape and strength of the line profile at each limb angle is the same in the "spots" as in the "photosphere." In our case, where we expect the spots to be virtually black anyway, this assumption is not critical, and much simplifies the computational process. It should be noted, however, that if the line equivalent width is different in the spot than it is in the photosphere, what we are really mapping is a combination of surface brightness and line strength. In cases in which the *shapes* of the spectral lines are dramatically different in the "spots" than in the photosphere, and in which both spots and photosphere make a significant contribution to the observed line, then some more elaborate prescription may need to be used. For our case, however, since the spot does not make a significant contribution to the observed flux, we set dI_λ/dI_c equal to I_λ/I_c (where I_c is the continuum surface brightness and the I_λ's are the specific intensities across the spectral line), which much simplifies the computing. A demonstration of the consequences of this simplifying assumption on the image solution will be given in § IV*f*.

The radial velocity of the zone due to rotation is then calculated. The appropriate values of dI_λ/dI_c across the line profile are then multiplied by the effective area of the zone and shifted in wavelength according to the correct radial velocity. These values then become the response matrix elements for the data pixels obtained at that phase for that particular zone on the star. They tell how changing the surface brightness of that particular zone on the star will affect the rotationally broadened line profile of the star at that particular phase. The entire transformation matrix, $\boldsymbol{R}$, consists of all these values, for each zone on the star and for each data phase. In Figure 2, we demonstrate what a small but otherwise realistic response matrix looks like, in more graphic form. In this case, the stellar surface has been divided into just 14 zones, each about 45° across, of which 11 are visible at some time. The data space consists of five phases, each of 40 data points per phase, so the matrix consists of 11 by 200 elements. Summing the individual R_{jk} elements over all the visible zones would produce five rotationally broadened line profiles, strung end to end, one for each phase.

Figure 3 shows a pictorial view of a response function matrix for a more realistic (but still fairly low spatial resolution) case involving 10 phases with 40 data points per phase, and 435 visible zones on the stellar disk. Each zone is about 9° across, and the stellar inclination is 45°. In this representation of the $\boldsymbol{R}$ matrix, the 400 point data direction again runs horizontally, and the 435 zone image direction runs down the vertical. The topmost row corresponds to zones at the visible pole, and zone numbers run sequentially down the figure. For display purposes, the local specific intensity profiles are represented here as emission features and the continuum is set to zero. So the bright "wiggly" lines denote relative contribution at any zone and data pixel to the total line flux equivalent width. The observed line flux profile is obtained by vertical summation for each phase, i.e., vertically collapsing the "wiggle" of each phase into a single summed profile at the bottom.

Several interesting features of this view of the $\boldsymbol{R}$ matrix deserve mention. The first is the increase of the range of excursion of any zone with increasing colatitude. For zones at or very near the pole (*top of figure*), the velocity excursion range is essentially zero, and the "wiggly lines" converge to line center

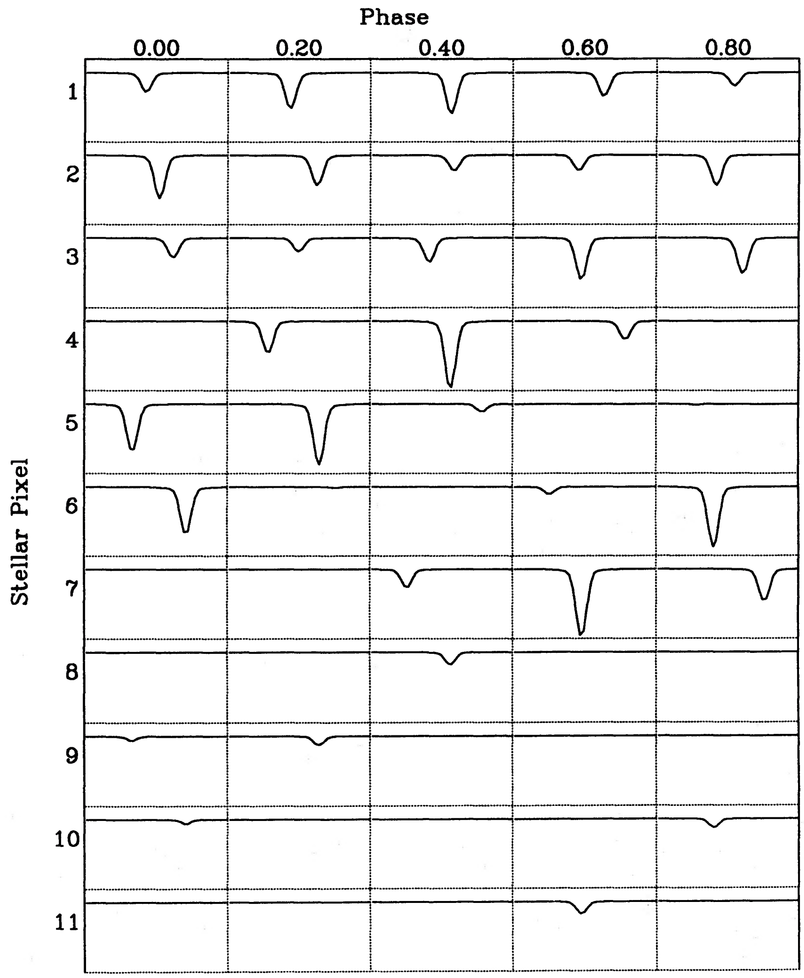

FIG. 2.—Schematic of a small but otherwise realistic transformation matrix. This one is for five phases, 40 data points per phase, and 11 visible zones on the star. The stellar inclination is 45°. The uppermost zone is nearest the stellar pole.

for all phases. As one moves along in zone number down the figure, one moves to lower latitudes on the star, and the amplitude of the wiggle increases. This functional dependency yields the latitude information in the final image. Second, zones that affect the line profiles the most (the brightest parts of the wiggles here) are those zones nearest the subobserver latitude and at disk center. As one moves toward the limbs, the contributions of any zone become less due to limb darkening and decreasing projected area. Third, the wiggles are continuous down to the point where zones are no longer circumpolar. Below here, any given zone passes out of view at the receding limb of the star for some time, before reappearing at the approaching limb. Thus, the wiggles become discontinuous. The increasing angle, which these discontinuities make with respect to the horizontal direction, arises from the fact that the number of zones per latitude band increases with decreasing latitude.

The transpose of the response function matrix $\boldsymbol{R}'$ is then calculated. The transpose is essentially an approximation to the true inverse of $\boldsymbol{R}$. It simply tells which image zones most affect which data pixels and is needed later by the maximum entropy inversion routines.

c) *Iterative Image Reconstruction*

We start the iterative reconstruction process with an initial guess at the stellar image, typically simply that the star is a uniform immaculate sphere. Each iteration then basically consists of comparing the "theoretical" profiles (calculated from the assumed image of the last iteration) to the "observed" profiles. The differentials between observed and theoretical line profiles result in many attempts to vary the surface brightness of many of the zones. For most zones, however, the changes cancel out, because positive changes needed at some phases will often be cancelled by negative changes at other phases. Only if the changes are all negative (i.e., at every phase) for a given zone will the code produce a cool spot. Also, the differentials have to be strictly in phase with the stellar rotation in order for the code to produce a spot. Thus the inversion method is reasonably insensitive to occasional weak line blends, given sufficient phase coverage, since these features are not phase-locked with the stellar rotation. The code generally recognizes and treats these spurious blends as noise. Each successive iteration takes typically slightly less than 3 minutes of cpu time on our VAX 11/780 and produces closer agreement

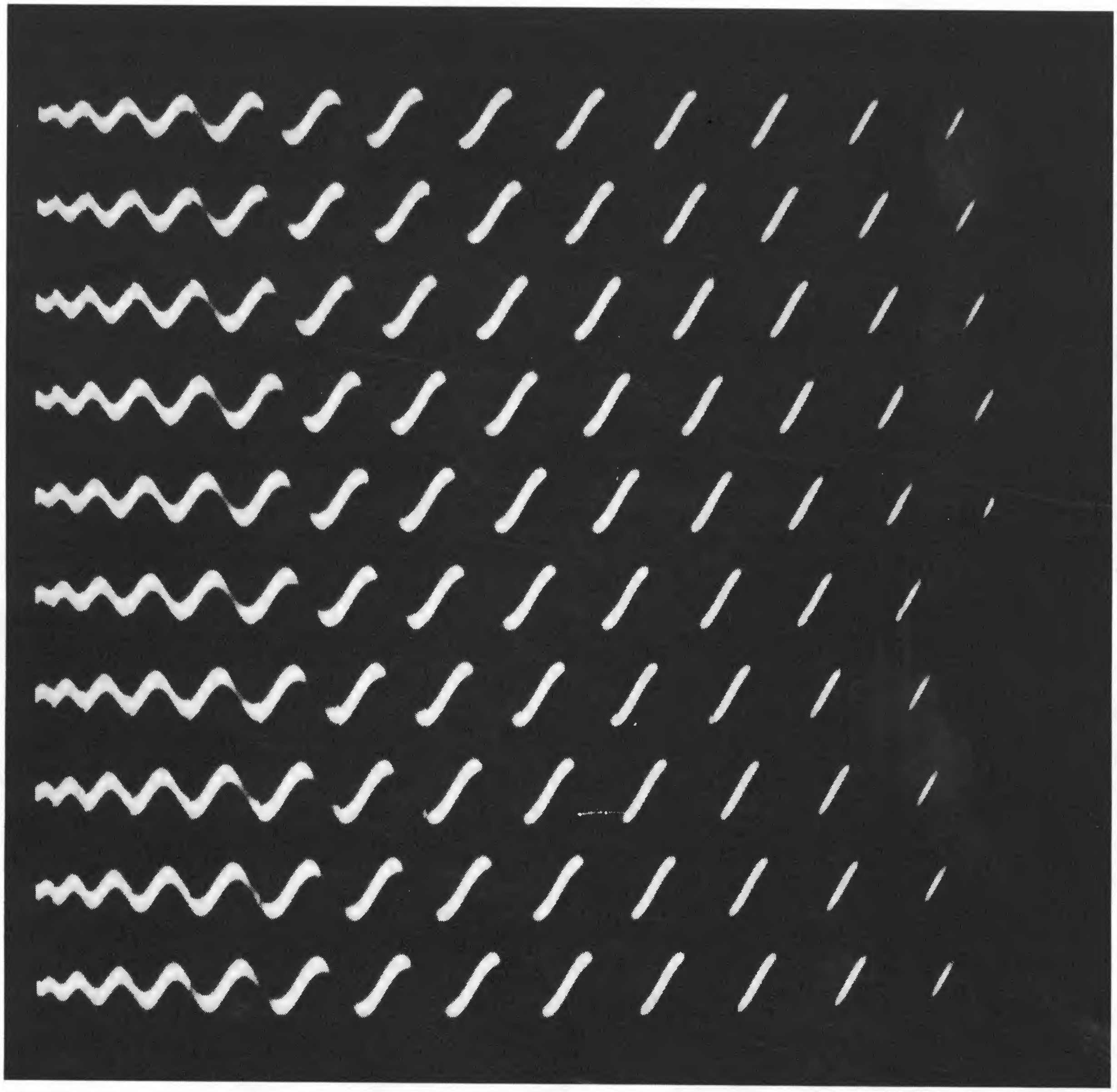

FIG. 3.—Actual transformation matrix for a situation involving 400 data points covering 10 phases, and 435 visible zones on a star seen at an inclination of 40°. The zone numbers run down the ordinate, with the pole at the top of the figure and the last visible zone at the bottom. The data direction runs along the abscissa. The brightness is roughly proportional to how much absorption a given zone produces in a given data pixel.

with the data. After about 10–20 iterations, the theoretical and observed profiles typically agree at the $S/N = 1000$ level.

The longitude of a spot is easily determined. It is just the phase at which the spot crosses line center. The longitude extent (width) of the spot is also easily found from the width of the corresponding bump in the line profiles. The latitude of a spot can be found from the speed with which the spot's bump moves across the line profile. Spots at high latitudes move very slowly and always stay near the center of the line profile. Spots at low latitudes move rapidly and over a larger range across the line profile. The latitude extent (height) of a spot is probably the most difficult thing to determine. There is a trade-off between temperature contrast and spot height. A tall warm spot and short cool spot tend to produce about the same size bump. This leads to some latitude smearing of the imaged features, as will be shown in the next section. However, both the solar analogy and starspot broad-band photometry suggest that starspot umbrae are quite cold, so this enables us to put some reasonable constraints on height.

The maximum entropy approach requires that the image quantity be always positive. This *positivity* requirement is handled in our case by setting up the problem such that the image quantity is surface brightness, which is of course always positive. Aside from this, there are no additional constraints set on spot temperatures. Thus our image solutions allow "hot" spots (regions higher in surface brightness than the normal photosphere) equally as well as "cool" spots.

IV. TESTS OF THE DOPPLER IMAGING METHOD

a) The "Vogtstar" Test

Our first test of the inversion process was to try the technique out on an artificial image of an RS CVn star. The $v \sin i$ of our artificial star is 40 km s^{-1} and its inclination is 40°, values typical of our real program objects. The spectral type of the artificial star was taken to be K1 IV ($T_{\rm eff} = 4750$ K), and the spectral line used to generate the synthetic data set was Fe I λ6430.

The test image chosen for this first case was a rather complicated image consisting of the letters V-O-G-T written in dark spots around our imaginary star. The test image of the "Vogtstar" is shown in Figure 4 for eight rotation phases. This image was then used to generate a data set of 16 line profiles of the Fe I λ6430 line at equidistant phases. For this and all subsequent tests, the synthetic data were generated using an explicit disk integration scheme, using a totally different zone geometry than that used in the reconstruction software, and with the true spectral line shape and strength appropriate for the dark spots explicitly included in the calculations. In this case, however, we made two assumptions intended to maximize the information in the line profiles. First, we assumed that the spectral resolution used was infinite, and second, we assumed that the spots were extremely cool, with $T_e \approx 2700$ K. Both effects tend to make the line profile variations rather more dramatic, and thus give the code more information to work with. Essentially, this case was intended to demonstrate just how well the image reconstruction software can work, in the best of all possible worlds.

The 16 profiles were assembled end-to-end into a 512 point data vector, and the Doppler imaging software was then given the appropriate physical parameters for the star (inclination, rotation velocity, and specific intensity profiles as a function of limb angle), and asked to derive an image of the star using only these synthetic line profiles. The input line profiles are shown in Figure 5 (*crosses*), and the fit to those profiles after 30 iterations of the inversion software is shown by the solid line. We let the program proceed until the profiles were fit to a very high level of accuracy.

FIG. 4.—Test input image of the "Vogtstar." Shown here are eight views of the star at equidistant phases. The phantom star at lower right illustrates the location of the rotational pole and inclination.

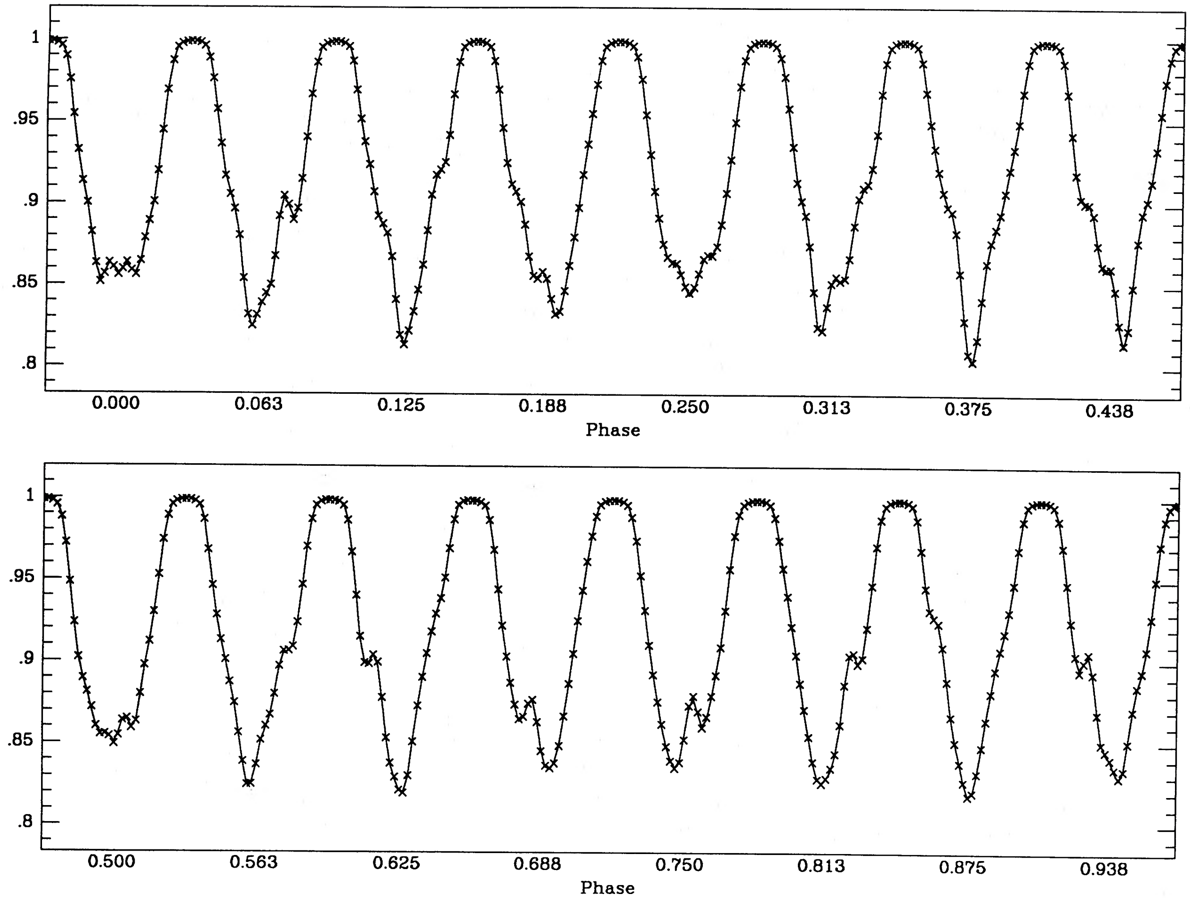

FIG. 5.—Synthetic spectral line flux profiles for the "Vogtstar" test image of Fig. 4. These flux profiles are for the Fe I line near 6430 Å at 16 equidistant phases. The theoretical profiles are shown as the crosses, and the inversion software's final fit (after 30 iterations) to these is shown by the solid line.

The image derived by the inversion process, also after 30 iterations, is shown in Figure 6 at the same eight phases as the input image and gives a good view of the level of the success of the inversion procedure. Though there is some loss of resolution, as expected, the test image has been recovered very well, certainly well enough to recognize all the letters, and to see a distinct difference between the "O" and the "G" letters. The effective resolution is approximately 12°. The recovered image is free from any systematic limb brightening or limb darkening effects, and also shows no systematic latitudinal brightening or darkening effects. Clearly, in this best of all worlds, the inversion software works very well.

In Figure 7 we show a series of pseudo-Mercator projections of the "Vogtstar" image solution at a selection of iterations, which gives a good idea of how the iteration proceeds. These maps show longitude as the abscissa and latitude as the ordinate, with the poles at top and bottom of each map and the equator in the middle. The iterative process clearly converges very rapidly on the main spot features. Within the first two iterations, the technique has correctly located all four of the letters. Within five iterations the basic size and approximate shapes of the spots have been derived, and further iterations basically serve only to improve the detailed shape and size information on the spots. Clearly, the main features of the solution are very well constrained by the data and do not rely heavily on entropy assumptions.

b) *The "Seven Spot" Test*

Our next test was to try the technique out on a simple but more realistic example. Our star is the same star as in the first test case, but in this case we have used a realistic spectral resolution of 125 mÅ, similar to what we normally use, and a spot temperature of 3300 K. The $v \sin i$ of our artificial star is again 40 km s^{-1}, and its inclination is again 40°. The test image in this case consisted of seven circular spots, including one spot pair separated longitudinally, one pair separated latitudinally, one pair diagonally, and a single isolated spot that was much smaller than our expected resolution element. The single small isolated spot was used not to test resolution, but rather to see if a feature smaller than our known resolution could even be detected. This "seven spot" test star image is shown in Figure 8 at eight equidistant phases. A set of 16 profiles of the Fe I λ6430 line was again generated at equidistant phases for this new test image, and the synthetic profiles and appropriate stellar parameters were passed to the reconstruction software.

The maximum entropy reconstruction of the "seven spot" test image is shown in Figure 9. The method has again recovered the correct image remarkably well. The very small spot is, as expected, unresolved and has a size consistent with our expected resolution element (~15°). However, the method has failed to recover the lower spot of the north-south pair and has produced a small amount of latitude smearing of the features.

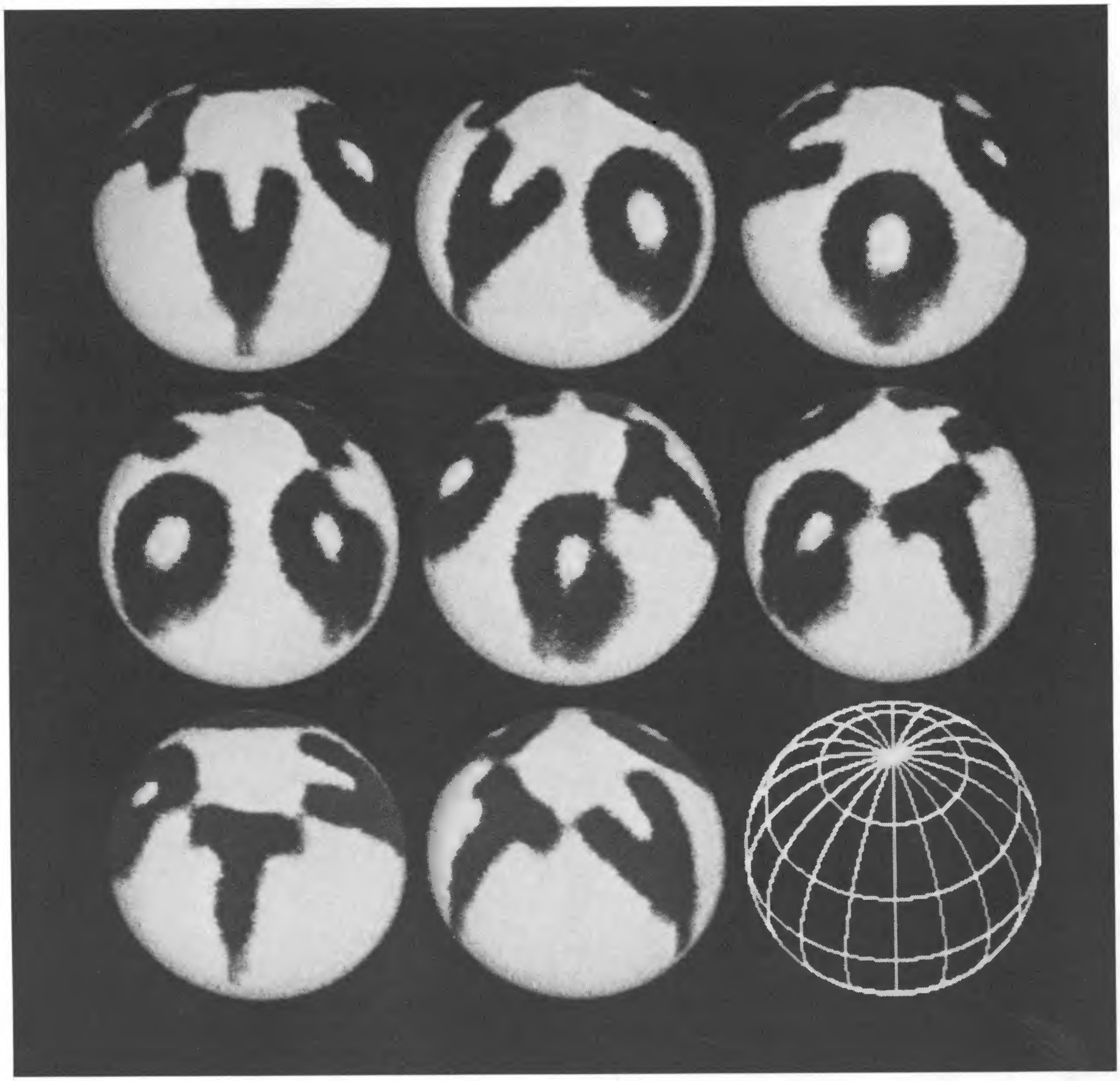

FIG. 6.—Doppler image recovery of the "Vogtstar" image of Fig. 4, from the synthetic line flux data of Fig. 5

Apparently, the lower spot is effectively being "shadowed" by the upper spot. Since the two spots are at the same longitude, they cross line center at the same time, and the signal from the lower spot is never clearly separable from that of the more visible upper spot. Were the star at somewhat higher inclination, the lower spot would, of course, be more visible since it does cross the stellar disk at a different rate than the northern spot and thus would produce an independent signal. However, at the low latitude of this simulation, the lower spot is not in view long enough for it ever to get very clear of the shadowing, and thus the program is only able to conclude that the northern spot has perhaps a southward-extending tail.

Latitudinal shadowing notwithstanding, the respective latitudes, longitudes, and sizes of the other spots are faithfully recovered, and there is no significant latitude bias as was evident in the results of Khokhlova and co-workers on Ap stars. And, unlike the traditional light curve modeling approach, which provides almost no unique information about spot shapes or locations, Doppler imaging determines both rather accurately.

c) *Initial Guess Effects*

The next question was to see how sensitive the technique is to the particular choice for the initial guess. We always use an immaculate star as the initial guess since it gets the initial profiles quite close to the data, and the solution converges rapidly. But we thought it possible that the inversion process might become unstable and divergent for other initial guesses, or that the final image may prove different for other initial guesses, a very dangerous situation if true. To test this, we started our initial guess with the Bright Star Catalog number of our favorite star, "1099," written in spots on the stellar surface. The data set and stellar parameters given to the reconstruction software were, however, the same as that used in our initial "Vogtstar" test. The inversion software was not fooled and in fact converged on the correct solution even faster than

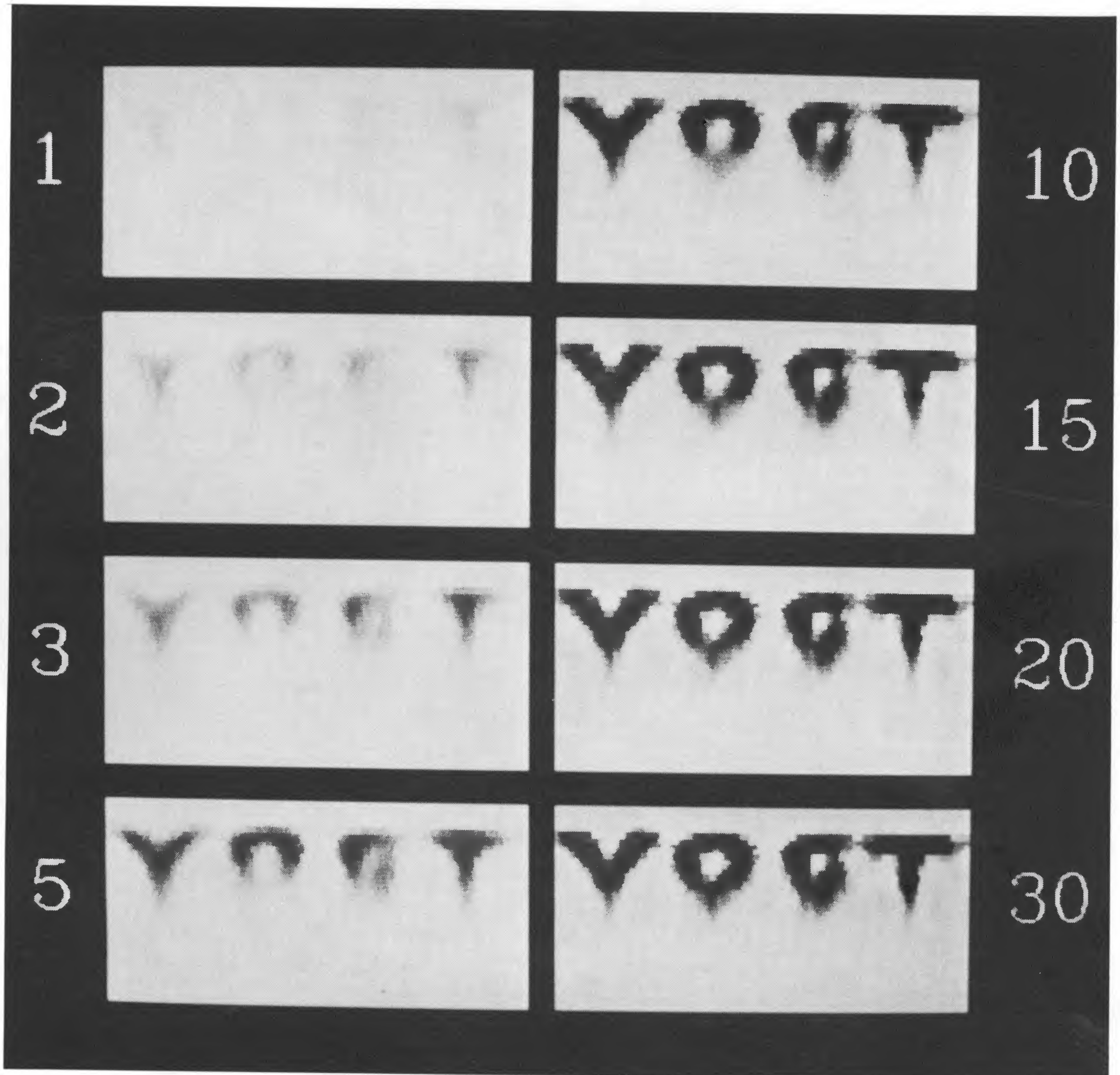

FIG. 7.—Pseudo-Mercator views of the "Vogtstar" solution of Fig. 6, showing progressive steps in the iteration process. Each map shows longitude as the abscissa, and latitude as the ordinate, with poles at top and bottom, and equator at the middle. Iteration numbers are listed to the sides of the views.

in the first "Vogtstar" test, since the "1099" initial guess, with four spotted regions already on the stellar surface, was actually a better guess than no spots. Figure 10 shows the initial "1099" guess image at the upper left (iteration 0), and various steps in the iteration, proceeding down the left-hand side, and continuing on at the top right. Within only two iterations the "Vogtstar" solution clearly dominates the image, and all evidence of the initial "1099" has been erased within four or five iterations. Clearly the reconstruction algorithm is quite robust, and the final solution in this case is quite independent of the initial guess.

One might argue that perhaps a more severe test would be to pick a spot distribution for the initial guess that was dramatically rather than subtly different from the known image. However, our present example tests an even more important point, that subtle details in the image are not lost or altered by starting with an approximately correct initial guess. Also, our standard immaculate star initial guess is, in itself, a dramatically different guess than any of our spot images and has always converged reliably. Though we have not formally proved it, we expect that, in general, final solutions will be quite insensitive to the initial guess. This insensitivity is just a consequence of the strong degree to which the solution is driven by the demand to fit the relatively large amount of very high quality data. The solution is strongly dominated by the χ^2 goodness-of-fit criterion rather than by the entropy maximization criterion. Incorrect initial guesses simply lengthen the convergence time of the iteration process.

Of course, if the code is given a completely nonsensical data set and/or an erroneous response function matrix, it becomes unable to converge to a solution. But it always does so gracefully. In such cases, it is obvious from the MEMSYS diagnostic information as the iteration proceeds that something is not correct. So while, the problem may be posed in such a way that

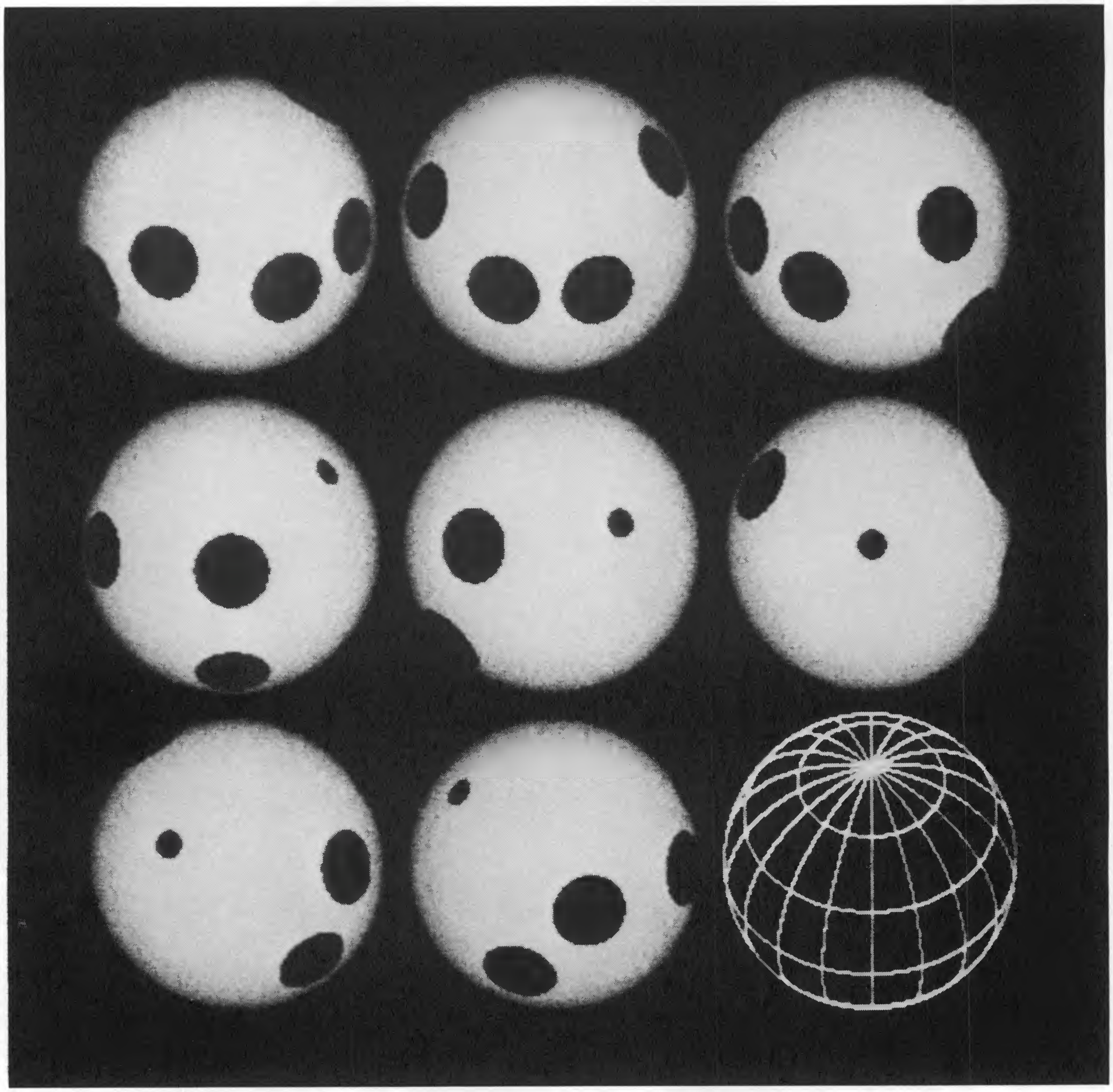

FIG. 8.—The "seven-spot" test image

the code is unable to find a solution, we have yet to see it give a false or misleading solution. The inverting routines seem remarkably robust in this respect.

d) *V* sin *i and Limb Darkening Effects*

The Doppler imaging technique is quite sensitive to getting the correct $v \sin i$ value for the star. It can thus be used to actually measure $v \sin i$'s very accurately by recognizing the signature that an incorrectly assumed $v \sin i$ leaves on the Doppler image, and choosing the $v \sin i$ value that minimizes or eliminates this signature. Choosing too small a $v \sin i$ for the matrix causes the code to produce a dark band completely encircling the star at about the subobserver latitude, while choosing too large a $v \sin i$ produces a bright band. In general, choosing a $v \sin i$ that differs from the true value by only 1–2 km s^{-1} at a $v \sin i$ of about 40 km s^{-1} will produce a very noticeable effect. In the cases of stars that have very distorted profiles, conventional techniques of determining the $v \sin i$ are often rendered ineffective, and we simply use the $v \sin i$ that produces the least systematic variation of surface brightness with latitude as the best guess for the true $v \sin i$.

Similarly, a wrong guess for the limb-darkening will also lead to a band around the star. If the star has more limb darkening than assumed in the construction of the matrix, for example, the code again produces a dark band circling the star at about the subobserver latitude. Hence, $v \sin i$ errors and limb-darkening errors (and errors in the limb variation of line strength) produce in general a very obvious systematic variation in surface brightness with stellar latitude. When such occurs, we usually correct by changing the $v \sin i$ to eliminate the bands, since this is the easiest parameter to change. However, in principle, errors in the chosen $v \sin i$ could just as well be attributed to errors in our limb-darkening or line-strength laws, although these are presumably known to reasonable accuracy from our atmosphere modeling. Fortunately, neither effect produces longitudinal variations in the surface brightness, as long as the phase coverage is fairly complete.

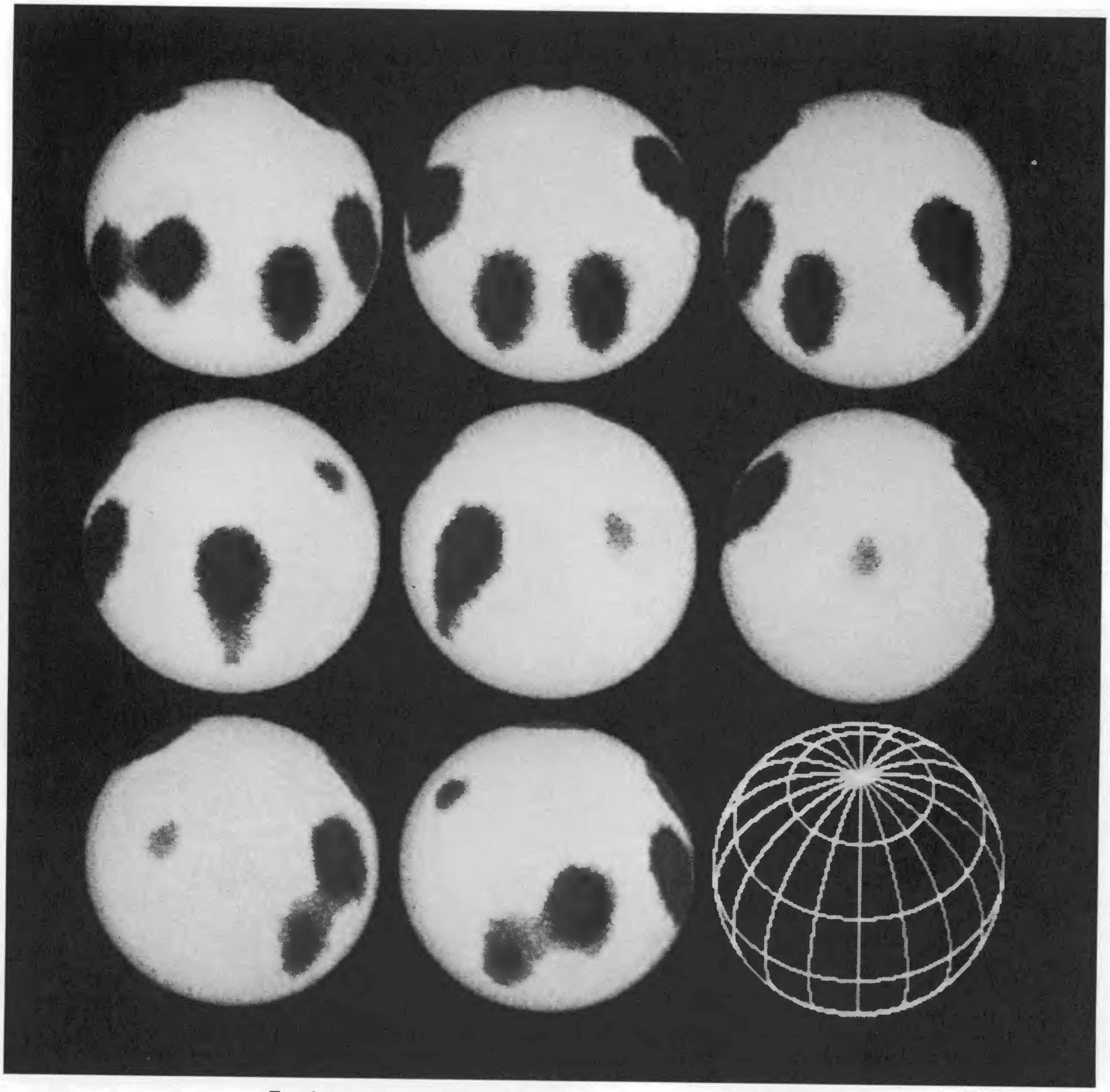

FIG. 9.—Doppler image recovery of the "seven-spot" test image of Fig. 8

e) *Inclination Effects*

Many stars that would be interesting to image are single stars, not members of binary systems. In such cases, the inclination is often unobtainable, or, at best, can only be roughly estimated from known rotation periods, the $v \sin i$, and an assumed radius. So, it is important to establish how sensitive the Doppler imaging technique is to uncertainties in the stellar inclination. We tested this by again using the "Vogtstar" test image, now with realistic spectral resolution and spot temperatures. However, we gave the inversion software the *incorrect* value of the inclination before computing the Doppler image. The true value of the inclination used to generate the data set for this case was 40°. To cover a reasonable range of inclinations, we passed incorrectly assumed inclinations of 20° and 70° to the reconstruction software.

The results of this test are demonstrated in Figures 11 and 12. At the top in Figure 11, we show the input "Vogtstar" image, viewed at the proper inclination. The middle pair shows the recovered image using an incorrect inclination of 20° but still viewed from a 40° angle. The bottom pair shows the recovered image using the correct inclination of 40°, and again viewed at the same 40° angle. In Figure 12, the top pair is a repeat of the previous 40° case for reference, and the middle pair shows the recovered image using an incorrect inclination of 70°, again viewed from a 40° angle.

In both the 20° and 70° cases of incorrectly assumed inclination, the image is still faithfully recovered. The 70° case yielded greater spot temperature contrast since, at this high inclination, the letters are quite foreshortened and thus must be made darker to account for the fixed heights of the line profile bumps. Likewise, the 20° case yields a much lower temperature contrast for the letters since they are less foreshortened and thus require less darkness to match the bump heights. The overall locations and shapes of the letters are, however, very well preserved and insensitive to errors in the assumed inclination. The bottom pair in Figure 12 shows the 70° solution again, but viewed equator-on to illustrate the fact that, at this

1987ApJ...321..496V

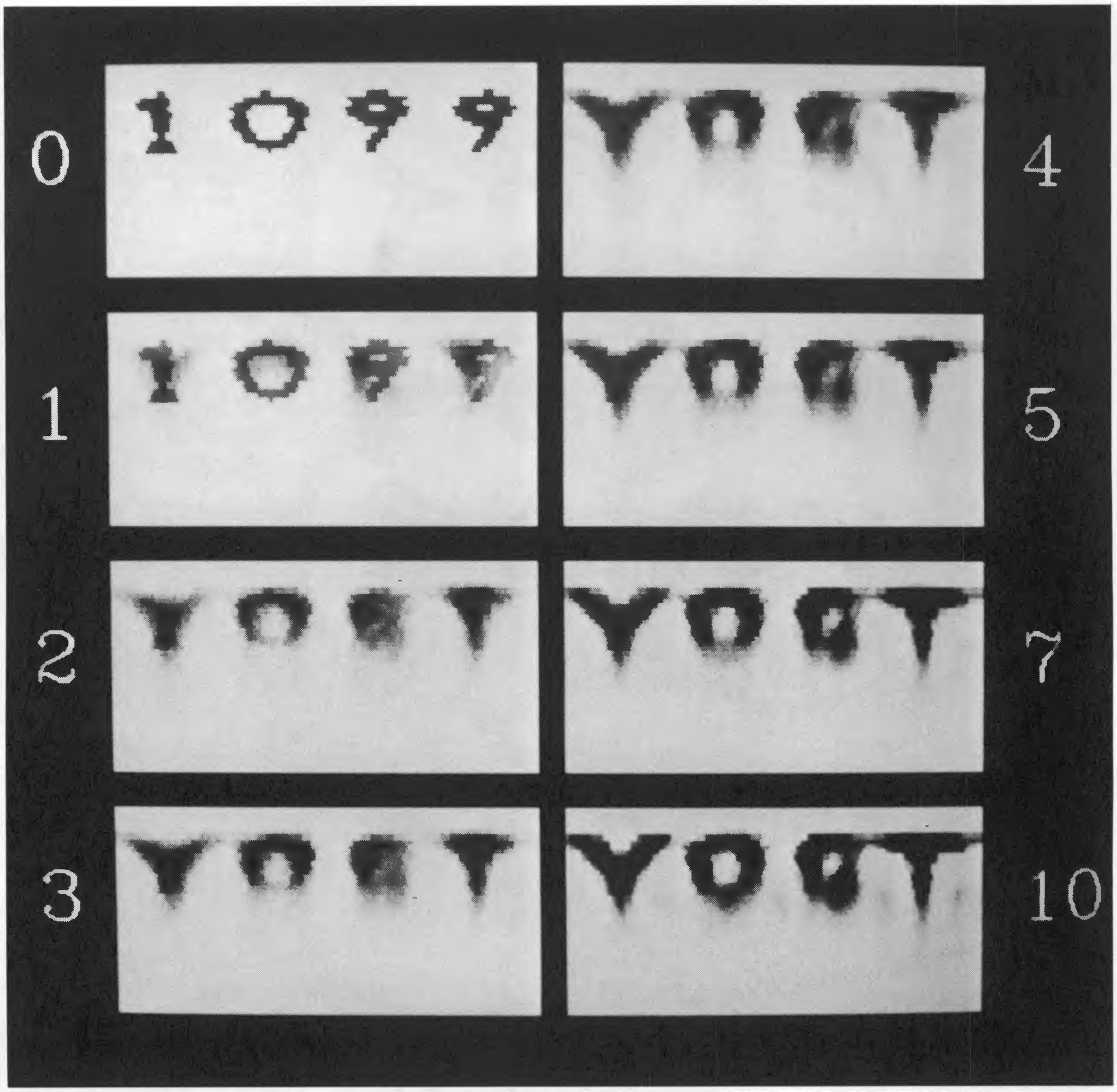

FIG. 10.—Pseudo-Mercator views of the effect of starting the iteration process with an incorrect initial guess. The initial "1099" image is shown at the upper left, and progressive iterations toward the solution proceed down the left, continuing on at the upper right. The final solution is shown at the lower right. Iteration numbers are listed to the sides of the views.

high of an inclination, the code puts weak mirror images of the spots in the wrong hemisphere. This "mirroring" is a result of the hemispheric ambiguity alluded to earlier. Essentially, the code minimizes the necessary spot contrast, and thus maximizes the entropy, by putting weak identical spots in both hemispheres, at the same longitudes but at opposite latitudes.

f) Effects of Finite Temperature Spots

We use an LTE–level of radiative transfer to account for variations in the specific intensity profiles and equivalent widths across the stellar disk. At present, for computational simplicity, we also assume that, at any given limb angle, the intrinsic line profile is independent of surface brightness, i.e., that the line profile is roughly the same in the spots as in the photosphere. In general, this assumption is not critical if the spots are effectively so cool that they contribute little flux. However, if the line profiles in the spots and in the photosphere are dramatically different, and the spots are sufficiently warm that they produce a finite contribution to the integrated absorption line, this assumption will be incorrect.

To gain some feeling for the sensitivity of our method to this assumption, we calculated a set of data strings for three different assumed spot temperatures: 3200 K, 3500 K, and 3800 K. For this test, we used the Ca I $\lambda 6439$ line, for which the line in the spot is much stronger than in the stellar photosphere. The line profile used in the spots was roughly 3 times as strong as that of the photosphere, and of course very much broader. This line profile was held constant at the three temperatures, so that the sole effect of increasing the spot temperature was to increase the relative surface brightness of the spots and to increase the contribution of the spot absorption to that of the integrated line profile. At a spot temperature of 3800 K, in fact, the spots contributed about 35% of the equivalent width of the observed absorption line, while at 3200 K the spots were effectively black. For this test the $v \sin i$ of the star was also increased to 80 km s^{-1}, to better illustrate the effect.

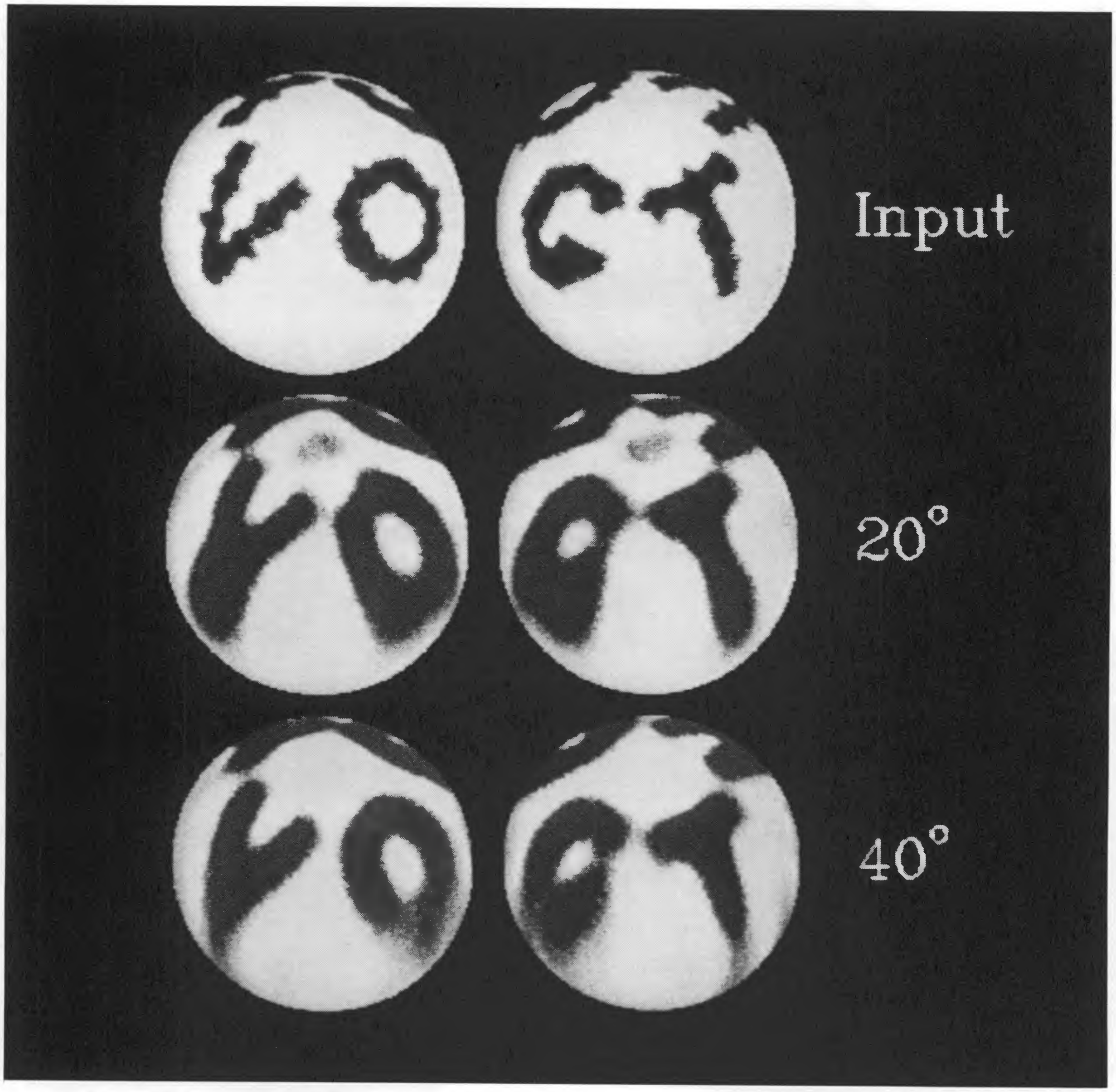

FIG. 11.—Inclination effects on Doppler images. Here, for clarity, each stellar image is shown in only two phases, 180° apart. All images are viewed from the correct inclination of 40°. Shown are (*top*) the input image with 40° inclination, (*middle*) the recovered image using an incorrect 20° inclination, and (*bottom*) the recovered image using the correct value of 40° for the inclination.

The result of this test is shown in Figure 13. The uppermost solution is for the very cold 3200 K spots. As expected, the code has no difficulty finding the V-O-G-T, since this case is essentially identical to those modeled earlier. The improved resolution of the letters is simply due to the higher $v \sin i$ used in the test; the number of resolution elements across the star is nearly linearly proportional to the rotation velocity, so the resolution is about twice as good as that in the earlier examples. In the middle solution, at a spot temperature of 3500 K, the very strong absorption line in the spots relative to that of the continuum almost perfectly cancels the lower surface brightness of the spots relative to the continuum, and the code has some difficulty finding the spots. Though the effect does not reproduce very clearly in the figure, what the code finds are relatively narrow dark letters surrounded by wider bright letters. This is exactly what might have been expected; the star is missing some narrow-lined absorption from the photosphere, but has excess broad-lined absorption from the spots. In the bottom frame, for a spot temperature of 3800 K, the product of spot brightness times absorption equivalent width becomes greater than the similar product in the photosphere, and the spots effectively look like bright spots to the code.

The poorer resolution in the bottom frame is due to the much greater line width of the line profile in the spots, resulting in fewer effective resolution elements across the star. Hence, in the bottom case, even with the very poor match between the physics assumed in making the transformation matrix (which uses only the photospheric specific intensity profiles) and the physics relevant to the data set, the code produces a relatively correct image. We conclude that the code is neither terribly

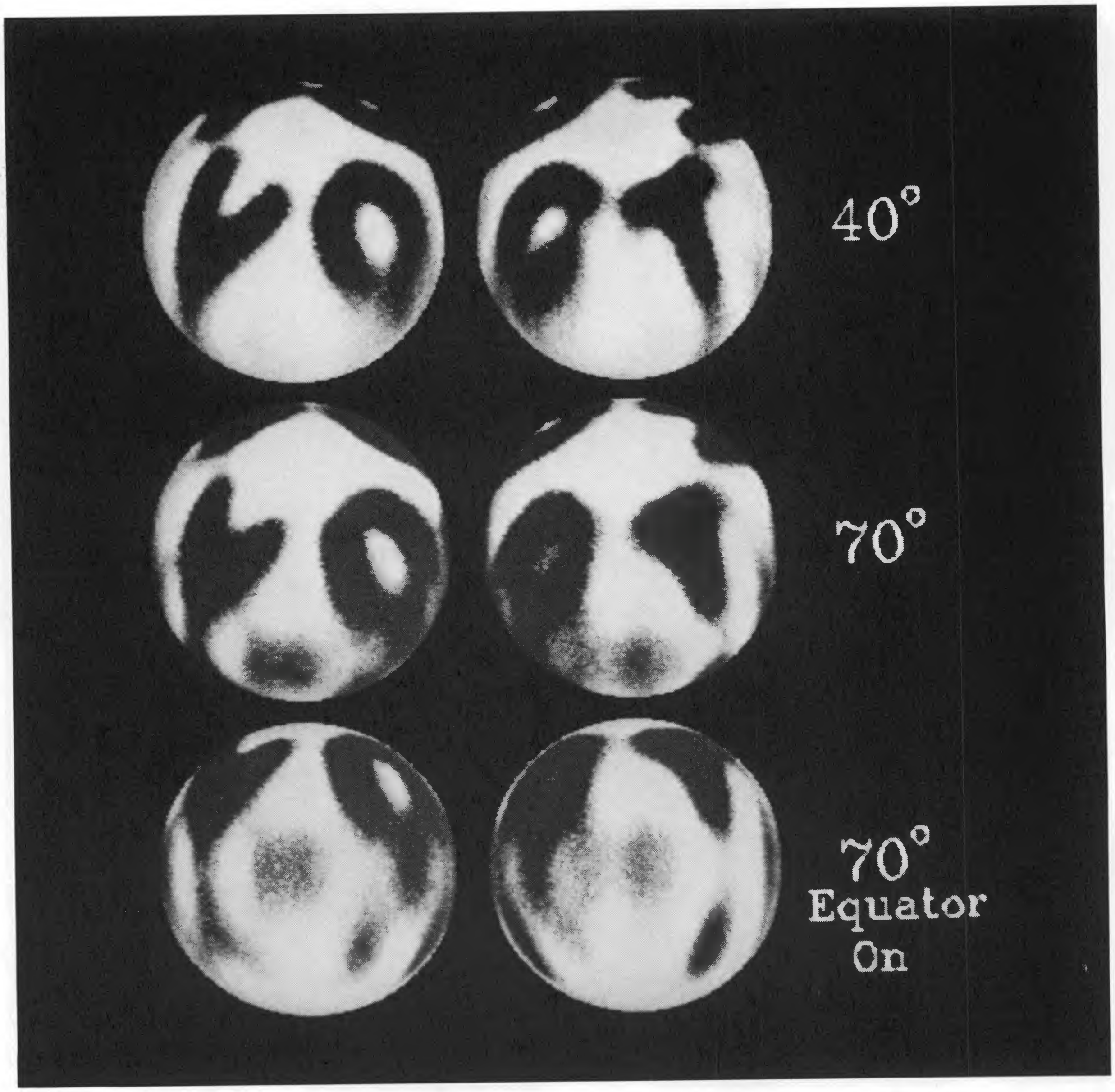

FIG. 12.—More inclination effects on Doppler images. Shown here are (*top*) the recovered image again using the correct 40° inclination and viewed at the correct angle, (*middle*) the recovered image using an incorrect value of 70° for the inclination, and viewed again at a 40° angle, and (*bottom*) the previous 70° solution viewed equator-on.

sensitive to our assumption of similar line profiles in the spots and photosphere, or indeed to any assumption about the intrinsic shapes of the local line profiles.

g) Signal-to-Noise Level Effects

It is of great interest to see how sensitive our Doppler images are to the signal-to-noise of the data set. In general, we try to keep S/N levels above 500 per resolution element on our brightest candidates, but as one goes fainter, or if the star is a rapid rotator (where exposure times must be short), much lower signal-to-noise ratios will be encountered. Here, the criterion of entropy maximization will become increasingly important, and the Doppler image will accordingly contain less information. To get an estimate of how quickly the image degrades with decreasing signal-to-noise ratio, random noise was added to the line profile set for the "Vogtstar" test case, and Doppler images then computed for a number of different noise levels.

The results are shown in Figures 14 and 15 for various values of S/N per pixel (where a pixel is set equal to half of our resolution element of 120 mÅ). Values of the signal-to-noise ratio of infinity, 500, and 300 are shown from top to bottom in Figure 14, and values of 300, 200, and 100 are shown in Figure 15. As expected, the contrast and resolution of the spots steadily decreases with decreasing S/N, and only in the highest S/N cases is the true shape of the spots recovered with any detail. However, even at the lowest S/N of 100 per pixel, the code finds only the four true spots and does a good job of determining their latitudes, longitudes, and sizes, and recovers some information about their general shapes.

By definition, the maximum entropy code produces the image with the least information required by the data, so even at the lowest S/N ratios the code should not produce spurious spots as long as the data uncertainties are properly treated, and this is true of the reconstructions. The principal effect of decreasing S/N is simply loss of effective resolution in the

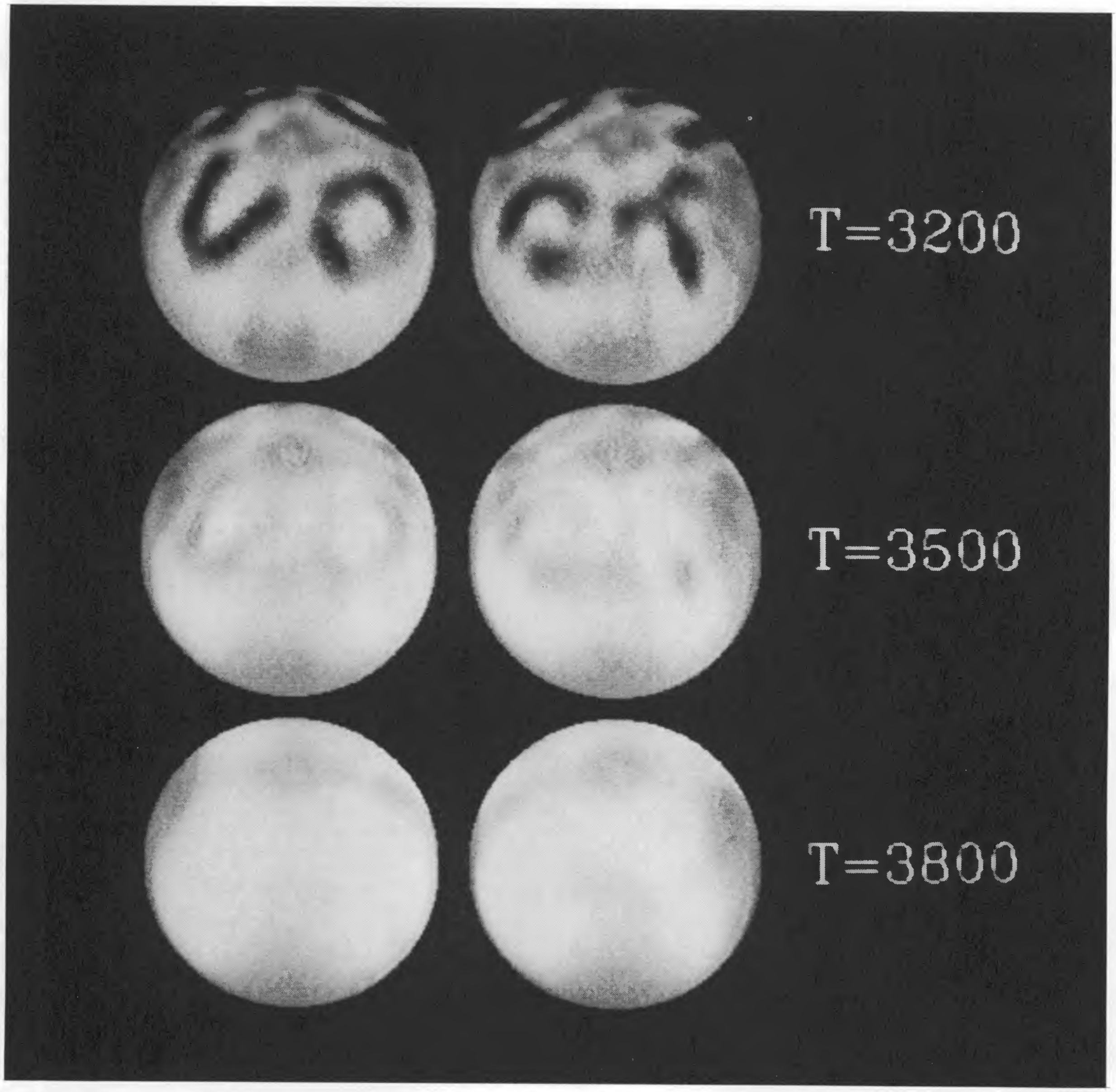

FIG. 13.—"Vogtstar" solutions when the absorption line (Ca I λ6439) is dramatically stronger in the spot than in the stellar photosphere. The stellar $v \sin i$ is 80 km s^{-1}. Data sets were constructed for three different spot temperatures: 3200 K, 3500 K, and 3800 K, using the same absorption line shape in the spot for all three. As the spot surface brightness increases, the spots change from dark, to effectively neutral, to "bright."

image, and a decrease in the required spot contrast. Since our data sets generally attain S/N ratios of 300 to 500, we conclude that, as long as the systematic effects due to line blends, telluric features, and gross instrumental glitches are minimized, we can recover fairly detailed information about spot shapes, sizes, and locations at an effective resolution of within 50% of the theoretical maximum.

h) *Incomplete Phase Coverage Effects*

Finally, it is useful to examine the effect that incomplete phase coverage has on derived images. The spotted RS CVn stars have spots which can change significantly over the course of several months, so the data used in creating an image must be obtained in a single observing season. Unfortunately, many of our program stars have very inconvenient periods, which beat with the length of a day, week, or month, making complete phase coverage rather difficult in the real world of cloudy nights and harried Time Allocation Committees. In general, our data sets often consist of at most 10–12 spectra, often containing one or more phase gaps of order 0.2 in phase.

To test the effects of such phase gaps in a realistic observing situation, we produced a data set, using the "Vogtstar" spot distribution, but with a realistic spot temperature of 3200 K and a realistic instrumental resolution of 120 mÅ, and with a data set consisting of only 10 phases. This data set had two large gaps of 0.19 in phase, one at the time the "T" crosses the disk center and the other as the "O" crosses disk center. Smaller gaps existed as well for the "V" and the "G." The image reconstructed from this data set is shown in Figure 16. The effect of poorer phase coverage is rather similar to that of poorer S/N, in that the primary loss is in the detailed resolution of the spot shapes. The spot locations and sizes are rather faithfully recovered, along with considerable shape information, but it is no longer possible to read all the letters.

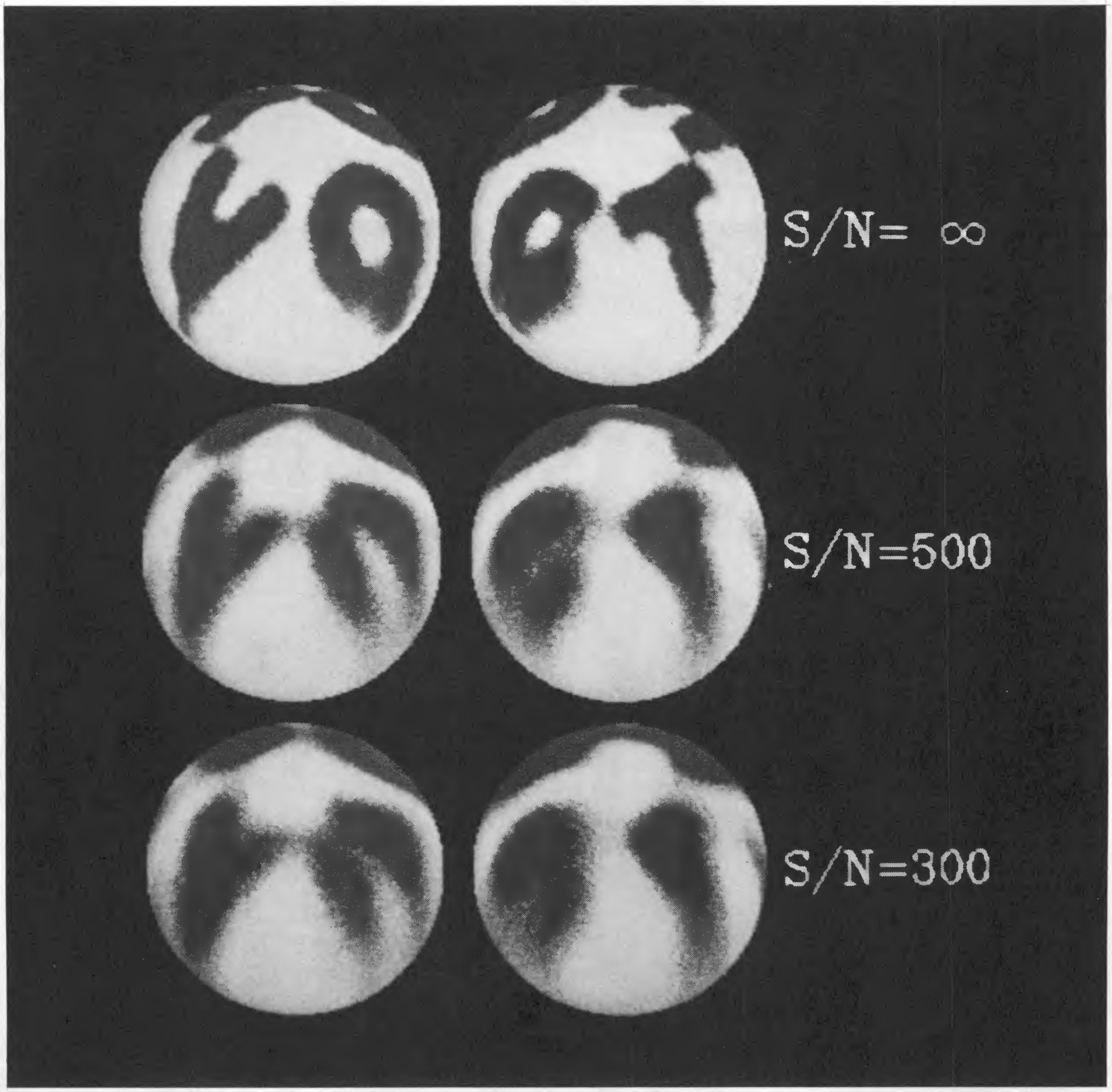

FIG. 14.—Views of recovered images of the "Vogtstar" for various signal-to-noise ratio levels of the line flux data. Shown are (*top*) infinite S/N, (*middle*) $S/N = 500$, and (*bottom*) $S/N = 300$.

The principle sources of information about the shapes of the letters is how the profiles change as the spots are carried across the disk. If one sees the spots at fewer angles, clearly much information is lost.

V. SUMMARY

We have shown that the technique of Doppler imaging, in its improved form, is a very powerful method for studying spots (or other features) on certain classes of rapidly rotating stars. Provided adequate amounts of high-quality spectral data can be obtained (a task well within the limits of present-day instrumentation and time allocations on large telescopes), angular resolutions of $\sim 15°$ or higher are readily achievable for real stars. For cool spotted stars, the Doppler imaging method is not very sensitive to errors or uncertainties in the assumed intrinsic shapes of specific intensity profiles. Other effects such as choosing the wrong inclination, having less than infinite S/N, and incomplete phase coverage only reduce the effective resolution somewhat, so that the detailed shape of a given spot is somewhat blurred. In all cases, however, the longitudes, latitudes, sizes, and rough shapes of the spots are recovered. In no cases are spurious spots produced by the reconstruction algorithm. In forthcoming papers, we will present applications of the Doppler imaging technique to the study of starspots on RS CVn and FK Com stars, and to the study of surface abundance distributions on Ap stars.

We would like to thank Dr. Keith Horne for bringing the MEMSYS software package to our attention, and to Dr. Steve Gull for kindly making it available. We are also very grateful to Dr. Robert Kraft and the Time Assignment Committee for making available over the past few years large amounts of observing time on the Shane 3 m telescope, in support of this project. This research was funded entirely by National Science Foundation grant AST-8210202, whose support we gratefully acknowledge.

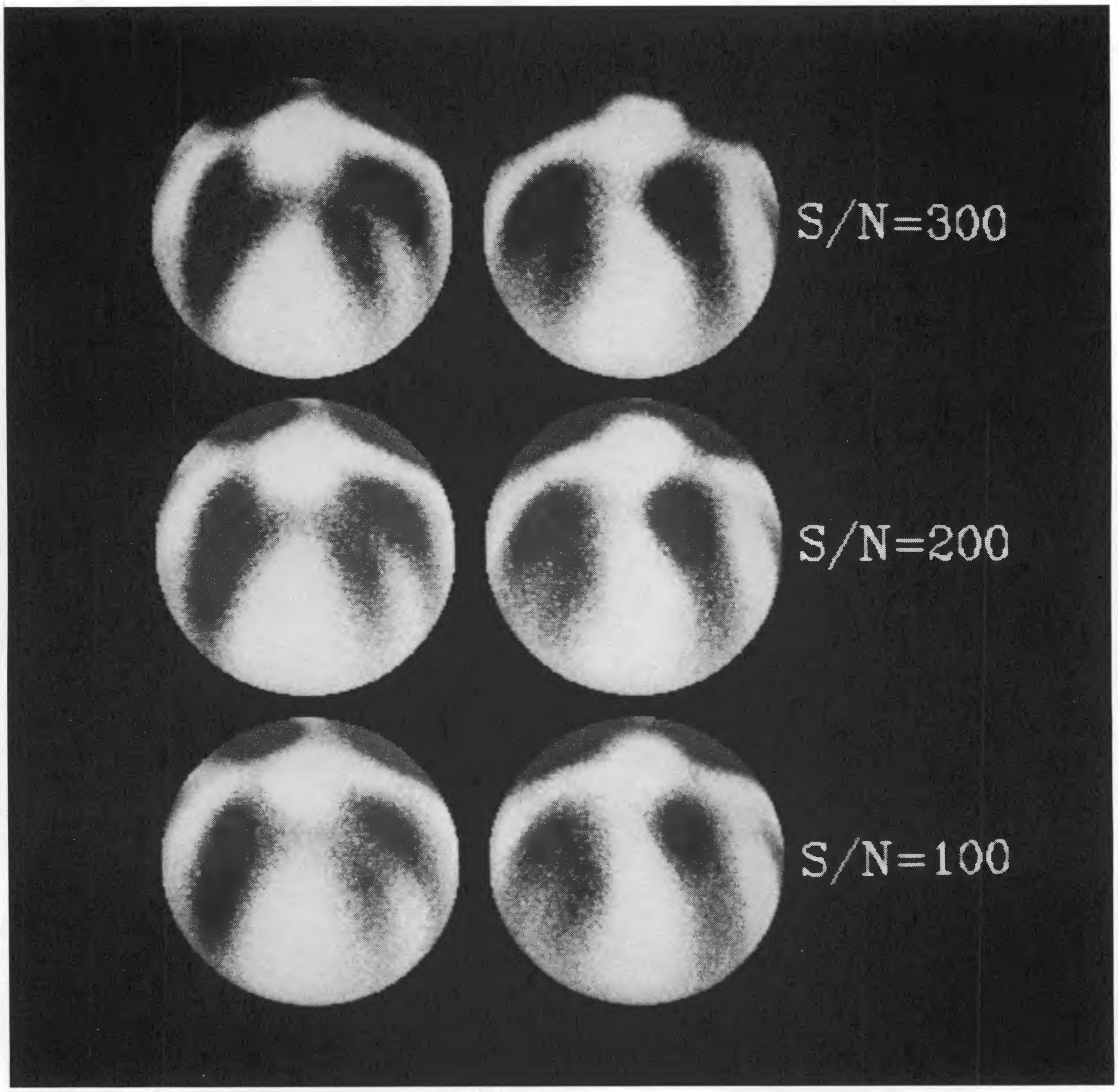

FIG. 15.—More signal-to-noise ratio level tests. Shown are (*top*) $S/N = 300$, (*middle*) $S/N = 200$, and (*bottom*) $S/N = 100$.

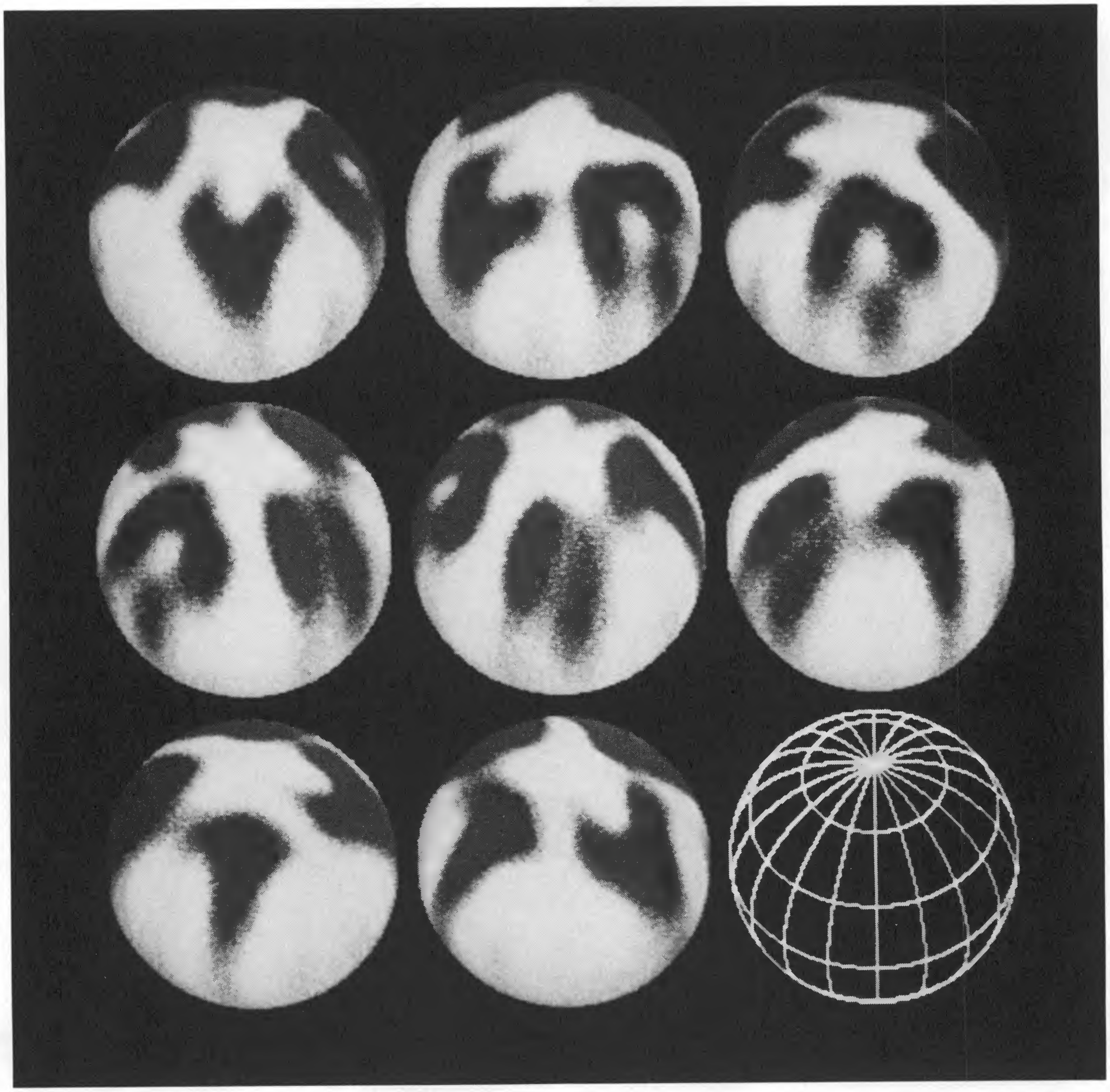

FIG. 16.—Effect of incomplete phase coverage on the solution. The image was derived using only 10 phases, with unequal spacing. The two largest phase gaps in the data set correspond to times when the "O" and "T" were crossing the center of the disk.

REFERENCES

Bell, R. A., Eriksson, K., Gustafsson, B., and Nordlund, Å. 1976, *Astr. Ap. Suppl.*, **23**, 37.

Deutsch, A. J. 1958, in *IAU Symposium 6, Electromagnetic Phenomena in Cosmical Physics*, ed. B. Lehnert (Cambridge: Cambridge Universtiy Press), p. 209.

———. 1970, *Ap. J.*, **159**, 985.

Falk, A. E., and Wehlau, W. H. 1974, *Ap. J.*, **192**, 409.

Goncharsky, A. V., Stepanov, V. V., Khokhlova, V. L., and Yagola, A. G. 1982, *Astr. Zh.*, **59**, 1146 (English trans. in *Soviet Astr.*, **26**, 690).

Gull, S. F., and Skilling, J. 1983, in *Indirect Imaging*, ed. J. A. Roberts (Cambridge: Cambridge University Press), p. 267.

Khokhlova, V. L. 1975, *Astr. Zh.*, **52**, 950 (English trans. in *Soviet Astr.*, **19**, 576.)

———. 1985, *Ap. Space Phys. Rev.*, **4**, 99.

Khokhlova, V. L., Rice, J. B., and Wehlau, W. H. 1986, *Ap J.*, **307**, 768.

Khokhlova, V. L., and Ryabchikova, T. A. 1975, *Ap. Space Sci.*, **34**, 403.

Kurucz, R. L. 1979, *Ap. J. Suppl.*, **40**, 1.

Megessier, C. 1975, *Astr. Ap.*, **39**, 263.

Pavola, V. M., Khokhlova, V. L., and Aslanov, I. A. 1977, *Astr. Zh.*, **54**, 979 (English trans. in *Soviet Astr.*, **21**, 554.)

Pyper, D. M. 1969, *Ap. J. Suppl.*, **18**, 347.

Shore, J. E., and Johnson, R. W. 1980, *IEEE Trans.*, **IT-26**, 26.

———. 1983, *IEEE Trans.*, **IT-29**, 942.

Skilling, J., and Bryan, R. J. 1984, *M.N.R.A.S.*, **211**, 111.

Vogt, S. S., and Penrod, G. D. 1982, in *IAU Colloquium 71, Activity in Red-Dwarf Stars*, ed. P. Byrne and M. Rodonò (Dordrecht: Reidel), p. 379.

———. 1983, *Pub. A.S.P.*, **95**, 565.

ARTIE P. HATZES, G. DONALD PENROD, and STEVEN S. VOGT: Lick Observatory, and Board of Studies in Astronomy and Astrophysics, University of California, Santa Cruz, CA 95064